Eur. Phys. J. B **50**, 593–602 (2006)
DOI: 10.1140/epjb/e2006-00181-2

THE EUROPEAN PHYSICAL JOURNAL B

High-frequency dynamics of Co/Fe multilayers with stripe domains

N. Vukadinovic[1,a], M. Labrune[2], and J. Ben Youssef[3]

[1] Dassault Aviation, 92552 St-Cloud Cedex, France
[2] LPMTM, CNRS-UPR 9001, Institut Galilée, Université Paris-13, 93430 Villetaneuse, France
[3] LMB, Université de Bretagne Occidentale, FRE 2697/CNRS, 29285 Brest, France

Received 25 January 2006
Published online 17 May 2006 –

Abstract. Within the framework of two-dimensional (2D) numerical micromagnetic simulations, the equilibrium magnetization configuration and the high-frequency (0.1–30 GHz) linear response of Co/Fe multilayers have been investigated in detail. Due to the perpendicular anisotropy of Co layers, a stripe domain pattern can develop through the whole multilayer, the characteristics of which depend on the magnitude of the perpendicular anisotropy, the respective thicknesses of Co and Fe layers and the number of Co/Fe bilayers in the stack. One of the most striking features associated with the layering effect is the ripening aspect of the static magnetization configuration across the multilayers which induces complicated dynamic susceptibility spectra including surface modes and volume modes strongly confined within the inner Fe layers. The effect of the cubic magnetocrystalline anisotropy of Fe layers and the influence of a nonuniform perpendicular magnetic anisotropy within the Co layers on the static and dynamic magnetic properties of Co/Fe multilayers are then analyzed quantitatively.

PACS. 75.40.Gb Dynamic properties – 75.60.Ch Domain walls and domain structure – 75.70.Cn Magnetic properties of interfaces (multilayers, superlattices, heterostructures)

1 Introduction

Artificially structured magnetic materials such as multilayered films, wire and dot arrays are very promising candidates for applications in the future high-density magnetic storage media and, magnetoelectronic and microwave devices. In this context, a full understanding of the high-frequency dynamics of such nanoscale magnetic structures is of prime importance. Knowledge of linear magnetic excitations existing in these magnetic systems with both geometric confinement and magnetic microstructure can be viewed as a first step in this request.

A large amount of work was devoted to spin-wave excitations in multilayered magnetic films in the 1980s and the early 1990s [1]. The collective modes existing in ferromagnetic/nonmagnetic and all-ferromagnetic multilayers were computed and analyzed in detail (spin-wave frequencies, modes localization) [2,3]. In particular, the roles of interface anisotropies and interlayer exchange coupling on the spin-wave frequencies were quantitatively described. However, these previous theoretical works are all based on the assumption of uniformly magnetized films within the multilayer stack, the static magnetization orientation being the same for each layer. This approximation is justified by the existence of a static magnetic field strong enough to eliminate the domain structure and is consistent with the experimental configurations of Brillouin light scattering and ferromagnetic resonance (FMR) techniques. This assumption is generally no more valid when one or several ferromagnetic layers exhibit a significant perpendicular anisotropy and when the low-field regime (below the saturation field) is considered. In this case, the magnetic ground state can indeed correspond to a nonuniform micromagnetic structure depending on the individual layer thicknesses. In the limit of a single layer with a perpendicular anisotropy, a well known example is given by the so-called stripe domain structure that develops above a critical thickness associated with the spin reorientation transition from in plane to out-of-plane magnetization [4,5]. Stripe domains were also observed by magnetic force microscopy (MFM) in various multilayer films with periodically alternating ferromagnetic and nonmagnetic layers such as Co/Pd [6], Co/Pt [7,8], Co/Au [9–11] and Co/Ru [12] systems, in all-ferromagnetic Co/Fe [13], $Fe_{81}Ni_{19}$/Co [14] and FePd multilayers [15] and, in ferrimagnetic/ferromagnetic bilayers [16]. A similar stripe domain pattern was also evidenced in ultrathin Co/Cu/(Fe/Ni)/Cu(001) magnetic sandwiches using Photoemission Electron Microscopy (PEEM) [17]. Furthermore, detailed analyses of the stripe domain structure within such multilayer films were

[a] e-mail: nicolas.vukadinovic@dassault-aviation.fr

performed by means of numerical simulations based on a 2D static micromagnetic model. Nice agreements were found between theory and experiments in terms of stripe periodicity, remanent magnetization and saturation field for Co/Pt [18] and Co/Au [19] systems (purely long-range dipolar interaction between the ferromagnetic layers) and, for Co/Fe [20] and FePd [15] (long-range dipolar interaction and short-range direct exchange coupling at each interface between the ferromagnetic layers).

On the other hand, the high-frequency response of stripe domain structures was studied both experimentally and theoretically for single layers. It was shown that FMR [21,22] and the zero-field high-frequency permeability spectra [23,24] exhibit multiple resonance lines. 2D dynamic micromagnetic simulations reproduce very well the main features of spectra and provide a deep insight on the localization of resonance modes by analyzing the spatial distribution of the dynamic magnetization within the stripe domains [23,24]. In addition, the roles played by the uniaxial perpendicular anisotropy [25], the film thickness [24], an in-plane polarizing magnetic field [24] and the orientation of the pumping field with respect to the stripe direction [25,26] on the high-frequency response were also investigated and nicely correlated with experimental data. Nevertheless, no results were reported to our knowledge concerning the magnetic excitation spectra of multilayers with stripe domains.

The aim of this paper is to investigate by means of numerical micromagnetic simulations the zero-field microwave response of multilayers supporting such a nonuniform micromagnetic structure and to highlight the new dynamic behaviors induced by the layered geometry. The considered multilayer films consist of periodic stacks alternating Co and Fe layers on a nanometer scale. This system was selected due to the large contrast of magnetic parameters, mainly in term of magnetic anisotropy, between the Co and Fe layers which reinforces the layering effect. After a brief description of the 2D dynamic micromagnetic model adapted for treating the linear response of multilayered structures, the layering effect on the main features of susceptibility spectra is investigated in detail. In particular, the roles played by the number N of Co/Fe bilayers, the influence of the cubic magnetocrystalline anisotropy of Fe layers and the effect of a nonuniform perpendicular anisotropy are outlined.

2 Key points of the dynamic micromagnetic model

The frequency dependence of the full dynamic susceptibility tensor $\overline{\overline{\chi}}$ is computed by using a two-dimensional (2D) micromagnetic model. This one, described elsewhere [25], is based on the solution in the frequency domain of the Landau-Lifshitz-Gilbert equation for magnetization motion linearized around the equilibrium configuration. The effective field $\mathbf{H}_{eff}$ incorporates the contributions from the exchange, anisotropy, demagnetizing, and dc applied magnetic fields. The magnetic systems are assumed invariant along one direction (z axis), periodic along the second direction (x axis) and of finite thickness along the third direction (y axis). This model is well adapted for probing the dynamic response of nonuniform and periodic equilibrium magnetization configurations as those encountered in single-layer films with stripe domains (the z axis coincides with the stripe direction) [23–25].

In order to treat the case of multilayer films with stripe domains, this model has been extended. Each magnetic layer i is described by its thickness t_i and the following magnetic parameters: the exchange constant A_i, the saturation magnetization $M_{S,i}$, one or several volume anisotropy constants $K_{\beta,i}$ ($\beta = 1, 2, ...$) according to the crystal symmetry, the gyromagnetic ratio γ_i and the Gilbert damping parameter α_i. Along the interface between two magnetic layers, denoted i and j, the following boundary conditions have to be fulfilled:

(i) the continuity of the direction of the magnetization (strong exchange coupling regime [27]), namely:

$$\mathbf{m}_i = \mathbf{m}_j \qquad (\mathbf{m}_\alpha = \mathbf{M}_\alpha / M_{S,\alpha}\,,\ \alpha = i, j), \quad (1)$$

(ii) the Rado-Weertmann [28] relation deduced from the minimization of the free magnetic energy density (surface contribution) which reads in the absence of interface anisotropy:

$$A_i \frac{\partial \mathbf{m}_i}{\partial \mathbf{n}} = A_j \frac{\partial \mathbf{m}_j}{\partial \mathbf{n}}, \quad (2)$$

where $\mathbf{n}$ is the normal to the interface.

For the two free surfaces, the last relation transforms into $\dfrac{\partial \mathbf{m}}{\partial \mathbf{n}} = 0$.

3 Micromagnetic simulations of the zero-field dynamic susceptibility spectra for Co/Fe multilayers

The all-ferromagnetic multilayer films under consideration consist of periodic stacks of Co/Fe bilayers with an additional Co layer on the top making the multilayers symmetrical with respect to the mid-plane ($y = 0$) as displayed in Figure 1. Thereafter, each stack is denoted $N(\mathrm{Co}_{t_{\mathrm{Co}}}\mathrm{Fe}_{t_{\mathrm{Fe}}})$ where N is the number of bilayers or the total stacking number and t_{Co} and t_{Fe} are, respectively, the thicknesses of individual Co and Fe layers in nanometers. The magnetic parameters used for the micromagnetic simulations are gathered in Table 1. These parameters are representative of cobalt [29,30] and iron [31,32] thin films at room temperature. For the sake of simplicity, two assumptions were made concerning the anisotropy energies:

(i) the prevailing contribution arises from the perpendicular uniaxial anisotropy of Co films characterized by the first-order anisotropy constant K_u. The adopted value, $K_{u,\mathrm{Co}} = 5 \times 10^6\,\mathrm{erg/cm^3}$, corresponds to the one of hcp Co films [33]. The effect of a nonuniform perpendicular anisotropy across the Co layers will be analyzed in Section 3.4.

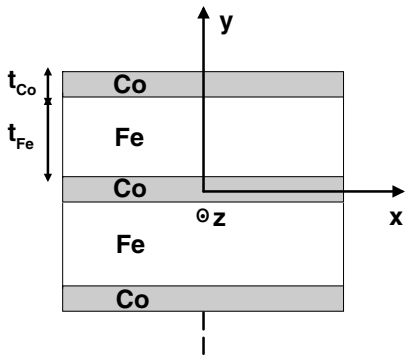

Fig. 1. Schematic representation of the multilayer geometry and coordinate system. The investigated multilayers consist of periodically alternating Co and Fe layers of respective thicknesses t_{Co} and t_{Fe}.

Table 1. Set of magnetic parameters for the Co/Fe multilayers used for the micromagnetic simulations.

	A (erg/cm)	M_s (emu/cm^3)	γ (s^{-1} Oe^{-1})	α
Cobalt	1.8×10^{-6}	1400	1.92×10^{7}	0.023
Iron	2.1×10^{-6}	1700	1.84×10^{7}	0.012

(ii) the iron layers are first assumed totally isotropic. The role played by the cubic magnetocrystalline anisotropy on the dynamic response of Co/Fe multilayers will be investigated in Section 3.3.

The static and dynamic micromagnetic simulations were performed using a spatial discretization with mesh sizes $\Delta_x \simeq \Delta_y \simeq 2.5$ nm lower than the exchange lengths for Co and Fe, $\Lambda_{\mathrm{Co}} = 3.8$ nm and $\Lambda_{\mathrm{Fe}} = 3.4$ nm, where the exchange length is defined as $\Lambda = (A/2\pi M_S^2)^{1/2}$. The dynamic susceptibility spectra displayed thereafter correspond to the in-plane diagonal elements of the dynamic susceptibility tensor (imaginary part) along the stripe direction χ''_{zz} (longitudinal configuration) and perpendicular to the stripe direction χ''_{xx} (transversal configuration) averaged over the periodic cell and computed within the frequency range 0.1–30 GHz.

3.1 Effect of the layering pattern

In order to analyze the effect of the layering pattern, let us consider a single Co layer, the 4(Co$_{15}$Fe$_{15}$) multilayer (five Co layers separated by four Fe layers, the individual layer thickness being equal to 15 nm) and, an effective single film whose magnetic parameters are the average of those of Co and Fe layers, the average of a value X being defined as $\langle X \rangle = [(N+1)\,t_{\mathrm{Co}}\,X_{\mathrm{Co}} + N\,t_{\mathrm{Fe}}\,X_{\mathrm{Fe}}]/[(N+1)\,t_{\mathrm{Co}} + N\,t_{\mathrm{Fe}}]$. The effective single film is denoted hereafter as $\langle 4(\mathrm{Co}_{15}\mathrm{Fe}_{15})\rangle$. The three samples possess the same total thickness $t = 135$ nm. Figure 2a shows the cross-sectional equilibrium magnetization configuration (m_x, m_y, m_z components) over one period of the stripe pattern for the three samples. For the Co layer, the static magnetization configuration consists of an open flux pattern with well defined up and down domains magnetized along the y direction (see m_y component) separated by a Bloch-type domain wall at the film center (see m_z component) and surrounded by Néel caps at the film surfaces (see m_x component). This configuration resembles the one described by Ebels et al. [34] for a cobalt single layer with $t = 100$ nm. The zero-field stripe period P_0 is equal to 200 nm.

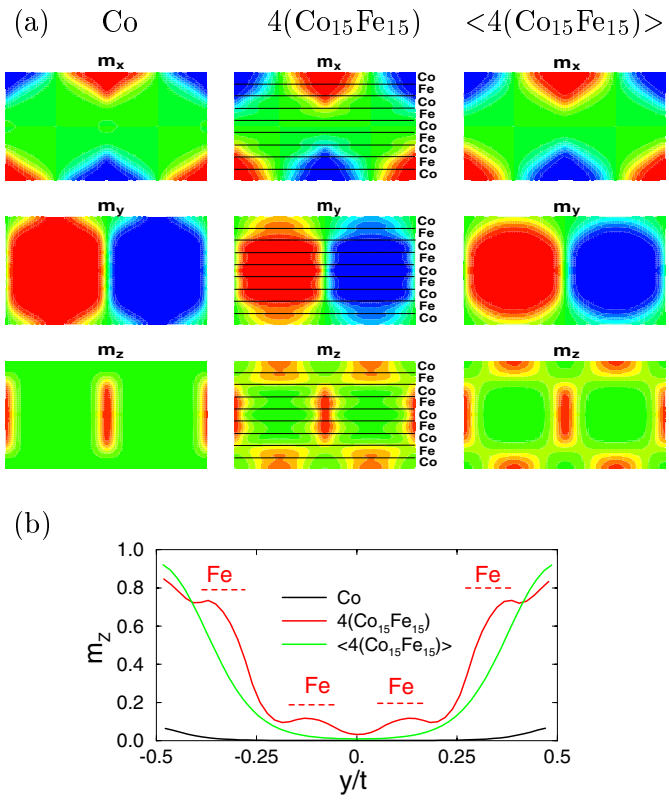

Fig. 2. (a) Equilibrium magnetization distributions over one period of the stripe pattern for the Co single layer, the 4(Co$_{15}$Fe$_{15}$) multilayer and, the $\langle 4(\mathrm{Co}_{15}\mathrm{Fe}_{15})\rangle$ effective single layer computed by 2D micromagnetic simulations. The magnetization components m_x, m_y and m_z are displayed in the plane (Ox, Oy) perpendicular to the stripe direction (Oz). The negative values appear in blue and the positive ones in red. (b) Longitudinal magnetization profiles $m_z(y/t)$ computed at the middle of the domain up (vertical slice in the map $m_z(x, y)$ at the position $x = P_0/4$) for the Co single layer, the 4(Co$_{15}$Fe$_{15}$) multilayer and, the $\langle 4(\mathrm{Co}_{15}\mathrm{Fe}_{15})\rangle$ effective single layer.

For the 4(Co$_{15}$Fe$_{15}$) multilayer, a more closed flux pattern is observed with a reduction of the m_y component near the surfaces of domains and correlatively an increasing m_z component within the same area. In these regions, the sign of m_z is unchanged between the two domains (unwinding surface magnetization distribution) which is the signature of the weak stripe domain structure [5]. With respect to the single Co layer, P_0 is increased and corresponds to 220 nm. These properties are also found for the effective single film. However, the most striking feature due to the layering pattern is the ripening aspect of the magnetization throughout the Co/Fe multilayer. This effect is clearly evidenced by representing the variation of the longitudinal magnetization component as a function

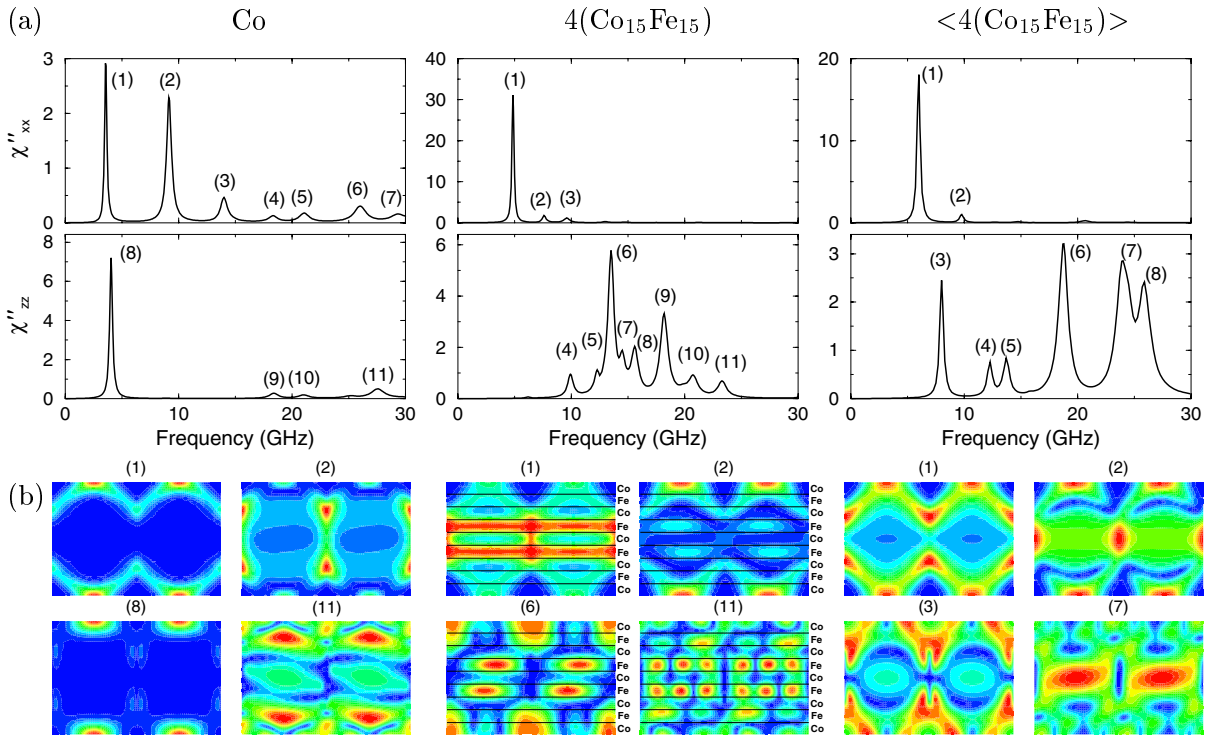

Fig. 3. Dynamic responses for the Co single layer, the $4(Co_{15}Fe_{15})$ multilayer and, the $\langle 4(Co_{15}Fe_{15})\rangle$ effective single layer. (a) Dynamic susceptibility spectra (χ''_{xx} and χ''_{zz} elements). (b) Spatial distributions of the dynamic magnetization $|\delta m_i(x,y)|$, $(i = x, z)$ over one period of the stripe pattern computed at the resonance frequency of different peaks (high levels in red and low levels in blue).

of the coordinate y (normalized by the total thickness t) along the stack normal for the position $x = P_0/4$ (middle of the domain up) (Fig. 2b). The m_z profiles have been drawn for the Co single film, for the $4(Co_{15}Fe_{15})$ multilayer and, for the effective single film. Although the amplitudes of variation of the longitudinal magnetization component are quite similar between the multilayer and the effective single film, an enhancement of m_z in the Fe layers is observed for the multilayer resulting in spatial oscillations of m_z across the stack. A detailed investigation of such static magnetization configurations in Co/Fe multilayers with different values of the perpendicular anisotropy constant and various individual layer thicknesses was recently reported [20]. Figure 2a reveals also a modulation of the domain wall width and the size of the closure area at the domain surfaces across the $4(Co_{15}Fe_{15})$ multilayer. These spin regions are shrinked within the Co layers and grown within the Fe layers.

The zero-field dynamic susceptibility spectra (χ''_{xx} and χ''_{zz} elements) for the Co single layer, for the multilayer and for the effective single layer are shown in Figure 3a. For the Co single layer, the main features of spectra can be summarized as follows:

(i) There exist multiple resonance peaks for both χ''_{xx} and χ''_{zz}. (ii) The magnetic excitations appear in a large frequency range from 3 GHz up to beyond 30 GHz and the mode positions are well separated. (iii) The transversal (χ''_{xx}) and longitudinal (χ''_{zz}) in-plane responses are of the same order of magnitude. (iv) The resonance modes are localized within different spin regions of the sample. The spatial distributions of the dynamic magnetization ($|\delta m_i(x,y)|$, $i = x, z$) over one period of the stripe pattern computed at the resonance frequency of some modes are displayed in Figure 3b. These maps indicate that the resonance lines (1) and (8) correspond to surface modes localized at surfaces of domains. The resonance lines (2) and (11) are associated with volume modes localized at the junction between the Néel caps and the Bloch domain wall and within some parts of domains, respectively. The aforementioned results present some similarities with those previously reported for a FePd single film [26] of approximately the same quality factor Q defined as $Q = K_u/2\pi M_S^2$ ($Q_{\mathrm{Co}} = 0.4$ and $Q_{\mathrm{FePd}} = 0.35$). The larger Co film thickness with respect to the one of the FePd film leads to an increasing number of resonance lines [23].

The dynamic spectra of the multilayer are deeply transformed (Fig. 3a). A predominant transversal response with a high-intensity and low-frequency peak (resonance line (1)) followed by two subsidiary peaks (resonance lines (2) and (3), respectively) is observed. The layering pattern affects drastically the structure of the main mode (Fig. 3b). The dynamic magnetization is indeed strongly confined within the innermost Fe layers and to a lesser degree inside the Bloch domain wall core at the film center. This mode confinement is intimately connected to the spatially inhomogeneous effective field distribution. As an illustration, Figure 4 shows the profile of the static effective field (y component) along the multilayer normal for the position $x = P_0/4$. Due to the

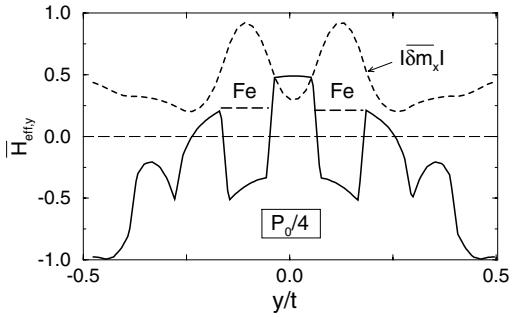

Fig. 4. Reduced static effective field profile $\overline{H_{eff,y}}(y/t)$ (solid line) computed at the middle of the domain up for the $4(Co_{15}Fe_{15})$ multilayer. The profile of the reduced dynamic magnetization $|\overline{\delta m_x}(y/t)|$ for the resonance mode (1) is indicated by the dashed line. The effective field (resp. the dynamic magnetization) is normalized by its maximum value.

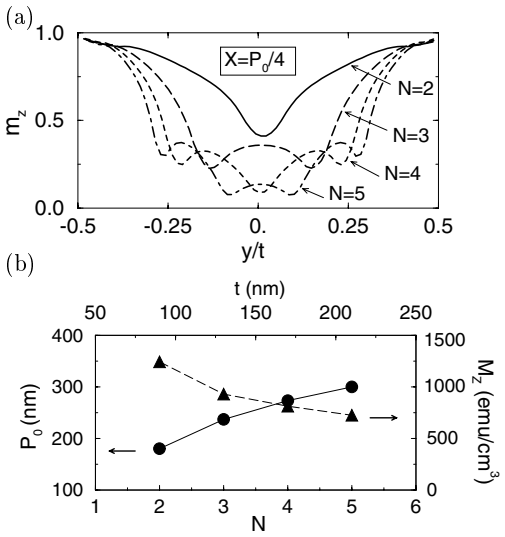

Fig. 5. Effect of the stacking number N on the static magnetization configuration of the $N(Co_{10}Fe_{30})$ multilayers, $N = 2$, 3, 4 and 5. (a) Longitudinal magnetization profiles $m_z(y/t)$ computed at the middle of the domain up. (b) N dependences of the zero-field stripe period P_0 and of the longitudinal static magnetization of the whole multilayer M_z.

adopted form of the anisotropy field (negative components along the x and z axes) [26], the predominant y component of the static effective field within the domain arises from the demagnetizing contribution due mainly to the surface and interface magnetic charges (discontinuity of the normal component of the magnetization between the successive media). This figure reveals a strong variation of the static effective field across the stack with positive values within the three innermost Co layers. For the resonance mode (1), the dynamic magnetization is localized inside the two Fe layers delimited by these Co layers with a large effective field value. Moreover, the dynamic effective field presents also an inhomogeneous structure across the multilayer due mainly to the large variation of the anisotropy field between the Co and Fe layers. It should be emphasized that this mode localization preferentially in the Fe layers is responsible for the relative weak linewidth of peak (1), the Gilbert damping parameter of Fe being assumed lower than the one of Co by a factor of 2, approximately. This effect combined with the reduction of the perpendicular anisotropy constant [35] explains the high amplitude of the main resonance line for the multilayer with respect to the one for the Co single layer. The resonance mode (2) appears clearly as a surface mode. By comparison to the Co single layer, the χ''_{zz} spectrum of the multilayer exhibits numerous resonance lines within the narrower frequency range 9–24 GHz. A detailed analysis of resonance modes reveals surface modes unaffected by the layering pattern, volume modes with a confinement within the inner Fe layers (see resonance mode (11)), and modes mixing both the surface and volume characters (see resonance mode (6)). Furthermore, it should be noted the nonuniform and periodic dynamic magnetization distribution within the Fe layers for the resonance modes (6) and (11).

To gain a better understanding of the evolution between the spectra of the Co single layer and those of the $4(Co_{15}Fe_{15})$ multilayer, it is instructive to consider the dynamic response of the effective film (Fig. 3a). As a result, the χ''_{xx} spectrum of the effective film bears ressemblance to the one of the multilayer with a predominant resonance line. The existence of such a spectrum is essentially related to the lowering of the perpendicular anisotropy constant with respect to the Co film. Nevertheless, the resonance frequency of the main peak does not coincide between the effective film and the multilayer and, as expected, the respective mode localization differs totally between the two samples. On the other hand, the χ''_{zz} spectrum of the effective film reveals also several resonance lines but appears quite distinct from the one of the multilayer in terms of mode position and mode localization. To summarize, the complicated dynamic response of the Co/Fe multilayer results from the contribution of two main effects, namely, a global one associated with the reduction of the perpendicular anisotropy of the whole multilayer due to the presence of Fe layers and a local one directly connected to the layering pattern and responsible for the mode confinement.

3.2 Effect of the stacking number

The stacks under consideration are made of Co/Fe bilayers with a repetition or stacking number N. This section is devoted to the N dependence of the dynamic susceptibility spectra. The $N(Co_{10}Fe_{30})$ multilayers are selected as a model system. According to the N value, two regimes can be distinguished. For $N = 1$, the magnetic ground state corresponds to an uniform in-plane magnetization for the whole multilayer. For $N \geqslant 2$, a stripe domain pattern occurs. The spin reorientation transition appears for a critical thickness t_c satisfying 50 nm $< t_c \leqslant$ 90 nm which corresponds in terms of Co thickness to 20 nm $< t_{c,Co} \leqslant$ 30 nm. This last value is consistent with the one for a single Co layer $t_{c,Co} \approx 25$ nm [33].

Figure 5a shows the longitudinal static magnetization profile across the stack (in reduced unit) for different N values, $N = 2$, 3, 4 and 5. These profiles are computed at the middle of the domain up. Increasing the stacking

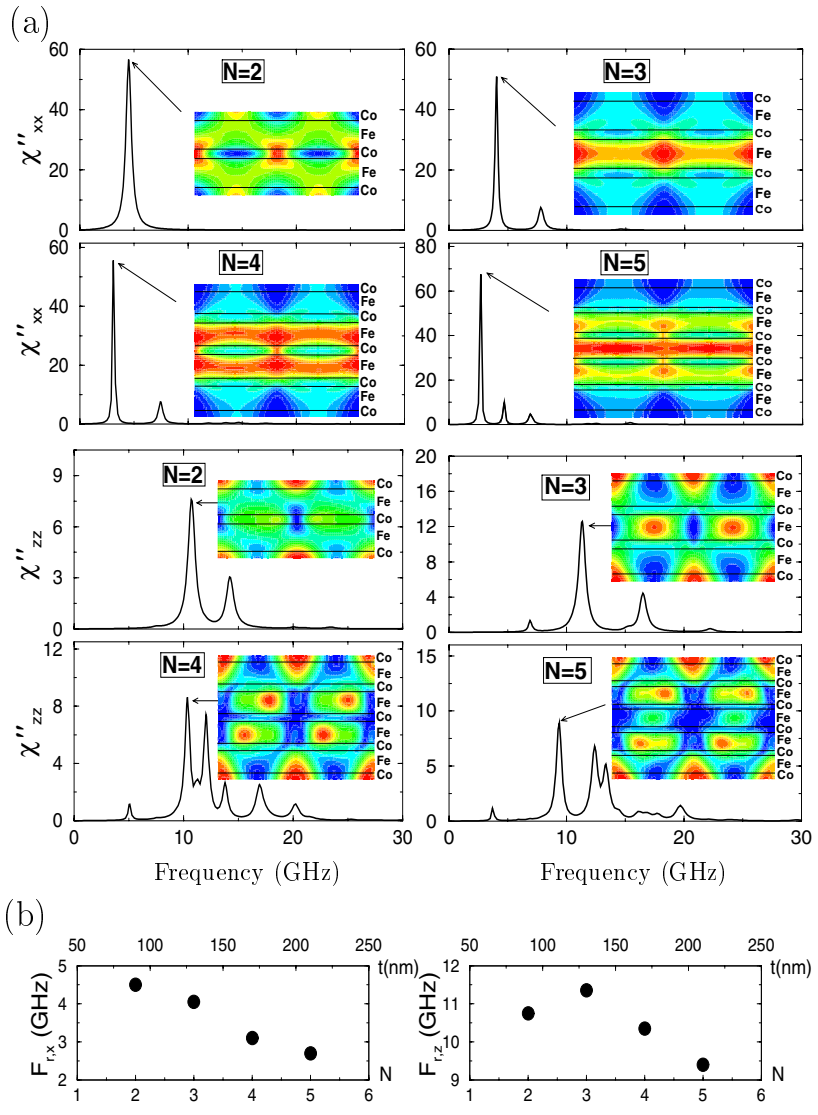

Fig. 6. Effect of the stacking number N on the dynamic response of the $N(Co_{10}Fe_{30})$ multilayers, $N = 2$, 3, 4 and 5. (a)χ''_{xx} and χ''_{zz} spectra. The color insets represent the maps of the dynamic magnetization over a periodic cell for the highest-intensity resonance line in the χ''_{xx} and χ''_{zz} spectra (high levels in red and low levels in blue). (b) N dependence of the resonance frequency for the highest-intensity resonance line in the χ''_{xx} and χ''_{zz} spectra.

number induces: (i) a decrease of the m_z component; (ii) an increase of the number of oscillations along the m_z profile. As shown in Section 3.1, these oscillations result from an enhancement of the m_z component within the Fe layers. For the $N(Co_{10}Fe_{30})$ multilayers, this effect is revealed only for the innermost Fe layers and is visible only for $N \geqslant 3$. The N dependences of the zero-field stripe period and the M_z component of the whole multilayer, $M_z = \sum_{i=1}^{2N+1} M_{S,i}\, m_{z,i}$, are displayed in Figure 5b. The zero-field stripe period is an increasing function of the stacking number and obeys a power law $P_0 \propto t^{\alpha}$, with $\alpha \approx 0.6$ as previously reported [19]. The M_z component of the multilayer decreases monotonously with increasing N.

The dynamic susceptibility spectra (χ''_{xx} and χ''_{zz} elements) for different N values are reported in Figure 6a. For both χ''_{xx} and χ''_{zz} spectra, increasing N yields the increase of the number of resonance lines. The χ''_{xx} spectrum is characterized by a high-intensity and low-frequency peak, and subsidiary peaks whose number is an increasing function of N. The maps of the main resonance mode for the different N values are given in the color insets (Fig. 6a). For $N = 2$, the dynamic magnetization presents high levels within the Bloch domain wall core, but some other spin regions of the whole multilayer exhibit a significant response. The confinement of the dynamic magnetization within the Fe layers appears for $N \geqslant 3$. Depending on the parity of N, the most excited Fe layers lie either at the multilayer center ($N = 3$ and $N = 5$) or within the innermost layers surrounding the central Co layer ($N = 4$). The resonance frequency of this main peak decreases monotonously with increasing N (Fig. 6b). The χ''_{zz} spectrum appears more complicated in particular for $N \geqslant 4$ with a wide frequency response and multiple sharp peaks. The analysis of the resonance mode for the the high-intensity peak shows a surface mode for $N = 2$ mainly localized within the Néel caps. For $N \geqslant 3$, the resonance modes keep a large value of the dynamic magnetization within the Néel caps and, in addition, present a confinement inside the inner Fe layers. The position of the most excited Fe layers evolves from the central layer ($N = 3$) to Fe layers more and more distant from the

center of the multilayer. The resonance of the main peak does not vary monotonously with increasing N (Fig. 6b). From these results, it appears that the N dependence of the susceptibility spectra recalls the thickness evolution of the dynamic response for a single layer [23]. However, the alternance of Co and Fe layers induces a confinement of the resonance modes in different Fe layers according to the value of the stacking number.

3.3 Effect of the cubic magnetocrystalline anisotropy of Fe layers

The above micromagnetic simulations were performed by neglecting the cubic magnetocrystalline anisotropy of the Fe layers. In this section, the effect of this cubic anisotropy on the equilibrium magnetization distribution and the dynamic susceptibility spectra is addressed. One relevant case reported in the literature [36] concerns the (Co/Fe) multilayers electron beam evaporated onto (100) Si single crystals. For such samples, grazing incidence X-ray reflectivity measurements revealed the existence of bcc (110) Fe and (0001) hcp Co layers. For a (110) Fe layer, assuming that the axes of the x, y, z coordinate system are parallel, respectively, to the $[1\bar{1}0]$, [110], and [001] axes, the cubic magnetocrystalline field reads (lowest-order term):

$$H_{K_1,x} = -\frac{2K_1}{M_S}\, m_x \left(1 - \frac{3}{2}m_x^2 - \frac{5}{2}m_y^2\right),$$
$$H_{K_1,y} = -\frac{2K_1}{M_S}\, m_y \left(1 - \frac{3}{2}m_y^2 - \frac{5}{2}m_x^2\right),$$
$$H_{K_1,z} = 0. \qquad (3)$$

For a positive K_1 value, the easy axis of magnetization lies along the [001] direction (z axis). This contribution has been incorporated in the effective field for both static and dynamic micromagnetic simulations. However, only the lowest-order term in the dynamic magnetization was retained for the computation of the linear dynamic response.

As an illustrative example, two (Co/Fe) multilayers exhibiting distinctive behaviors were investigated, namely, the $2(Co_{10}Fe_{30})$ and $4(Co_{15}Fe_{15})$ stacks. For each case, three values of K_1 were considered: $K_1 = 0$, 2.25 and 4.5×10^5 erg/cm^3. This last value is representative of the lowest-order cubic magnetocrytalline anisotropy constant for iron at room temperature [37]. Figure 7a shows the K_1 dependence of the profile $m_z(y/t)$ computed at the middle of the domain up. For the $2(Co_{10}Fe_{30})$ multilayer, increasing K_1 leads to an enhancement of m_z in the whole stack. Within the Fe layers, the magnetization is pulled by the cubic anisotropy along its preferential z axis. The direct exchange coupling between the Co and Fe layers causes the magnetization in the Co layers to be also canted towards the z axis. In contrast, the m_z profile is very weakly modified by the cubic anisotropy for the $4(Co_{15}Fe_{15})$ multilayer. In this last case, the slight variations of m_z are localized within and in the vicinity of the Fe layers.

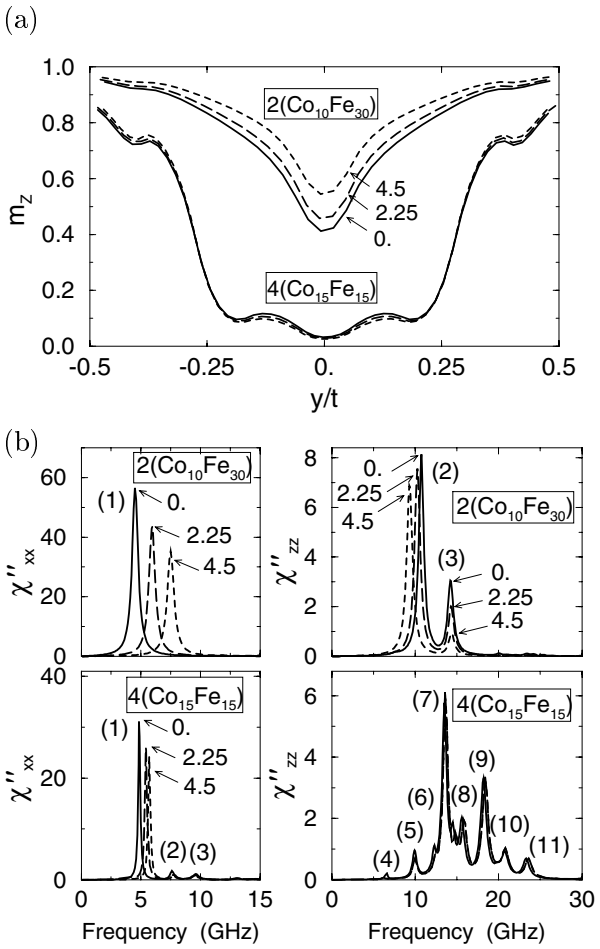

Fig. 7. Effect of the cubic magnetocrystalline anisotropy of Fe layers on the static and dynamic behaviors of the $2(Co_{10}Fe_{30})$ and $4(Co_{15}Fe_{15})$ multilayers. (a) Longitudinal magnetization profiles $m_z(y/t)$ computed at the middle of the domain up. Three values of K_1 are considered: $K_1 = 0$, 2.25 and 4.5×10^5 erg/cm^3. (b) K_1 dependence of the χ''_{xx} and χ''_{zz} spectra.

The consequences on the dynamic susceptibility spectra are reported in Figure 7b. For the transverse configuration (χ''_{xx} spectrum), increasing K_1 results in a shift of the main peak (resonance line (1)) towards the high frequencies whereas its amplitude (maximum value of χ''_{xx}, denoted hereafter as $\chi''_{xx,max}$) is reduced. The amplitude of these variations are mainly controlled by the stacking number and the Co/Fe thickness ratio. For the $2(Co_{10}Fe_{30})$ multilayer, the resonance frequency of the line (1) varies significantly and obeys a linear law as a function of K_1. On the other hand, only a slight and non linear increase of the resonance frequency with K_1 is observed for the $4(Co_{15}Fe_{15})$ multilayer. It should be underlined that for a (110) Fe single layer uniformly magnetized along the z axis, the resonance frequency of the gyroresonance scales as ${H_{K_1}}^{1/2}$ and $\chi''_{xx,max}$ as ${H_{K_1}}^{-1/2}$ for $H_{K_1} \ll 4\pi M_S$. For the longitudinal configuration (χ''_{zz} spectrum), two different behaviors can be reported. For the $2(Co_{10}Fe_{30})$ multilayer, the resonance frequency of the line (2) is lowered and the peak amplitude decreases as

K_1 increases. The cubic anisotropy does not affect significantly the position of the resonance line (3) but its amplitude decreases rapidly with increasing K_1. For the $4(Co_{15}Fe_{15})$ multilayer, the χ''_{zz} spectrum remains praticallly unchanged as a function of K_1.

As shown in Section 3.2, the resonance mode (1) for the $2(Co_{10}Fe_{30})$ multilayer results from the excitation of spin regions within the whole multilayer. Increasing K_1 transforms progressively the resonance mode (1) into a surface mode. For the $4(Co_{15}Fe_{15})$ multilayer, the resonance mode (1) is characterized by a strong confinement of the dynamic magnetization within the inner Fe layers (Fig. 3b). This mode structure is conserved over the range of investigated K_1 values. It should be keep in mind that the above reported results of static and dynamic micromagnetic simulations are related to multilayers with a prevailing perpendicular anisotropy of Co layers and a moderate cubic anisotropy with a z easy axis of Fe layers ($K_{u,Co}/K_1 \approx 11$).

3.4 Effect of a nonuniform perpendicular anisotropy of the Co layers

The micromagnetic simulations presented in the above sections are partly based on the existence of a volume anisotropy energy within each layer characterized by a space-independent anisotropy constant. This description is well adapted to represent the bulk magnetocrystalline anisotropy of Co and Fe layers. However, the origin of the perpendicular magnetic anisotropy (PMA) in the Co/Fe multilayers is still an open question. Broadly speaking, several major sources of PMA in magnetic multilayers have been identified [38] such as the mechanical stresses, the surface and interface roughness, the Néel anisotropy due to the symmetry breaking at the interface between the layers and, the interface diffusion. For the specific case of the Co/Fe multilayers, a semi-quantitative analysis has shown that the magneto-elastic effect originating from the lattice mismatch at the Co/Fe interfaces and the surface and interface roughness account partly for the PMA experimentally observed [20]. Moreover, the respective weight of these mechanisms is intimately related to the growth technique (molecular beam epitaxy, electron beam evaporation, rf sputtering) and the preparation conditions (pressure, growth temperature, deposition rate) of the multilayers. Incorporation of such mechanisms into the micromagnetic simulations requires to take into account their preferential localization in the vicinity of the Co/Fe interfaces. In this context, two stategies can be adopted. The first one consists in the introduction of the surface and interface anisotropy energies into the exchange (Rado-Weertman) boundary condition [28]. The effect of these surface and interface energies on the dynamic properties of multilayers in the saturated state was analyzed in detail and leads to significant changes in the spin-wave frequencies [2]. The second approach, adopted in this paper, describes the effect of surface and interface anisotropies by a volume contribution localized near the surfaces and interfaces and hence takes into account the finite spatial extent of these anisotropies. In other words, a profile $K_{u,Co}(y)$ must be incorporated in the micromagnetic simulations. It should be noted that the effect of different profiles of perpendicular anisotropy on the spin-wave spectra (saturated regime) in inhomogeneous garnet films were investigated in the past [39]. As an illustration, the case of $4(Co_{15}Fe_{15})$ multilayers exhibiting a multiple number of interfaces was selected. The magnetic parameters are the same as those reported in Section 3.1 except for the constant value of $K_{u,Co}$ replaced by the profile $K_{u,Co}(y)$ defined as follows: a large value of $K_{u,Co}$ is assigned to discretization cells in the Co layers adjacent to the Fe layers. This large value of $K_{u,Co}$ spreads over one mesh size, namely, $\Delta y = 2.5\,\text{nm}$. The inner cells of the Co layers possess a lower $K_{u,Co}$ value. For the sake of simplicity, the same profile is considered for the external Co layers (no distinctive treatment between the Co/Fe and Co/vacuum interfaces). Figure 8a shows three different stepwise variations of $K_{u,Co}$ within a given Co layer. These profiles satisfy the constraint relation $\sum_{i=1}^{6} K_{u,Co,i}\,\Delta y_i = 7.5\ \text{erg/cm}^2$. The differences

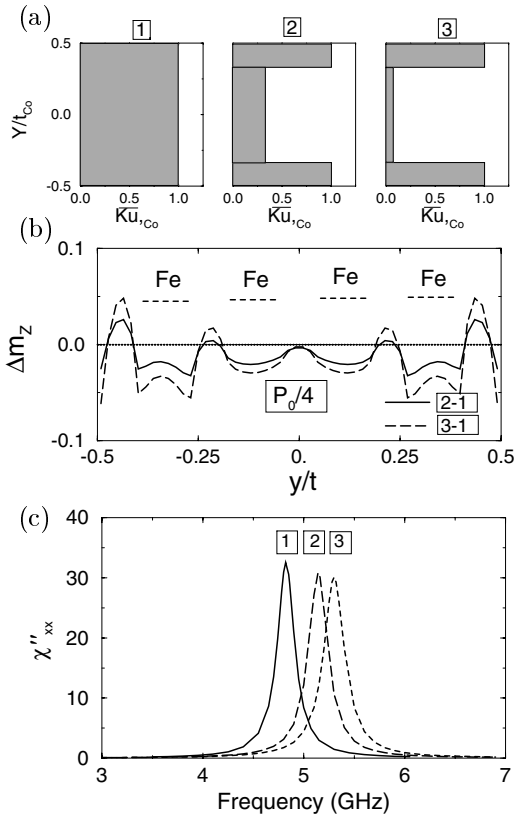

Fig. 8. Effect of a nonuniform perpendicular anisotropy of the Co layers on the static and dynamic behaviors of the $4(Co_{15}Fe_{15})$ multilayers. (a) Reduced perpendicular anisotropy profiles $\overline{K_{u,Co}}(y/t_{Co})$ across a Co layer. The perpendicular anisotropy constant K_u is normalized by its maximum value within the Co layers. (b) Variations of the longitudinal magnetization profiles $\Delta m_z(y/t)$ computed at the middle of the domain up. The reference corresponds to the profile displayed in Figure 2b (uniform $K_{u,Co}$ value). (c) χ''_{xx} spectra for the three perpendicular anisotropy profiles.

between the equilibrium longitudinal magnetization profiles (the reference is the case with a uniform $K_{u,\mathrm{Co}}$ value) computed at the middle of the domain up are drawn in Figure 8b. As expected, nonuniform $K_{u,\mathrm{Co}}$ values result in a decrease of m_z in the region of Co layers with a high value of $K_{u,\mathrm{Co}}$ and an increase of m_z at the center of the Co layers (low value of $K_{u,\mathrm{Co}}$). However, the last property vanishes when passing from the external Co layers to the central one. Inside the Fe layers, the m_z component is reduced due to the direct exchange coupling at the interfaces between the Co and Fe layers through the boundary condition (Eq. (2)). Increasing the constrast of $K_{u,\mathrm{Co}}$ leads to an enhancement of the variation Δm_z . The global quantities P_0 and M_z are slightly reduced when increasing the inhomogeneity of $K_{u,\mathrm{Co}}$. As shown in Figure 8c, the transverse susceptibility spectra is also changed by the introduction of the profile $K_{u,\mathrm{Co}}(y)$. The main resonance line is shifted towards the high frequencies when the contrast of $K_{u,\mathrm{Co}}$ is increased. The mode structure with a strong confinement within the two innermost Fe layers exists for each anisotropy profile. However, increasing the contrast of $K_{u,\mathrm{Co}}$ promotes a more and more nonuniform dynamic magnetization profile within these Fe layers (maximum value at the layer center).

4 Summary and conclusion

The static and dynamic magnetic properties of Co/Fe multilayers have been investigated using 2D numerical micromagnetic simulations. In such a model system, the existence of a perpendicular anisotropy within the Co layers can result in a stripe domain structure depending on the magnitude of the perpendicular anisotropy, the respective thicknesses of Co and Fe layers and the number of the Co/Fe bilayers in the stack. With respect to a single Co layer with the same total thickness, the layering effect induces a reduction of the perpendicular anisotropy and the emergence of spatial oscillations in the equilibrium magnetization distribution across the stack.

The dynamic susceptibility spectra over the frequency range 0.1–30 GHz associated with the Co/Fe multilayers reveal multiple resonance lines including surface modes and, for a sufficiently large number of bilayers, volume modes exhibiting a strong confinement within the inner Fe layers. This mode confinement originates from the large spatial inhomogeneity of the effective field distribution across the stack. These simulations represent the ideal case where the perpendicular anisotropy of the Co/Fe multilayers is thought to arise from the bulk magnetocrystalline anisotropy of the Co layers. Although the interpretation of the perpendicular anisotropy in such stacks is still lacking, it seems reasonable to suggest that the interface properties (mechanical stresses, roughness, interdiffusion) contribute significantly to the perpendicular anisotropy. Introduction in the micromagnetic simulations of a nonuniform perpendicular anisotropy preferentially localized near the Co/Fe interfaces has been performed and can be viewed as a first attempt to describe more realistic anisotropy profiles. As a result, the inhomogeneity of the perpendicular anisotropy can lead to frequency shifts of the main resonance lines.

Further investigation on this subject would need to gain quantitative information on the nature of the Co/Fe interfaces. Results of microstructural studies [36] obtained in the case of electron beam evaporated Co/Fe multilayers have shown the existence of sharp interfaces that give rise to a single phase magnetic behavior for the multilayer. In this case, a description of the magnetic interfaces by means of a direct exchange coupling via the boundary condition, as made in this paper, seems appropriate. The situation is probably different for sputtered Co/Fe multilayers for which diffuse interfaces can be expected. In this case, introduction of indirect exchange coupling [27] between Co and Fe layers in the static and dynamic micromagnetic simulations in order to account for the imperfect interfaces could be considered. Finally, due to the large number of parameters in such multilayered systems, it seems necessary in the future to compare the dynamic behaviors predicted by micromagnetic simulations with experimental ones (FMR, zero-field microwave permeability measurements) for Co/Fe multilayers in the unsaturated regime.

References

1. R.E. Camley, R.L. Stamps, J. Phys.: Condens. Matter **5**, 3727 (1993)
2. B. Hillebrands, Phys. Rev. B **41**, 530 (1990)
3. R.L. Stamps, B. Hillebrands, Phys. Rev. B **44**, 5095 (1991)
4. A. Hubert, R. Schaefer, *Magnetic Domains* (Springer, Heidelberg 1998)
5. M. Labrune, J. Miltat, J. Appl. Phys. **75**, 2156 (1994)
6. J.R. Barnes, S.J. O'Shea, M. Welland, J.-Y. Kim, J.E. Evetts, R.E. Somekh, J. Appl. Phys. **76**, 2974 (1994)
7. R.L. Stamps, L. Lovail, M. Hehn, M. Gester, K. Ounadjela, J. Appl. Phys. **81**, 4761 (1997)
8. L. Belliard, J. Miltat, V. Kottler, V. Mathet, C. Chappert, T. Valet, J. Appl. Phys. **81**, 5315 (1997)
9. S. Hamada, N. Hosoito, T. Ono, T. Shinjo, J. Magn. Magn. Mater. **198–199**, 496 (1999)
10. S. Hamada, N. Hosoito, T. Shinjo, J. Magn. Soc. Jpn **68**, 1345 (1999)
11. O. Donzelli, D. Palmeri, L. Musa, F. Casoli, F. Albertini, L. Pareti, G. Turilli, J. Appl. Phys. **93**, 9908 (2003)
12. S. Hamada, K. Himi, T. Okuno, K. Takanashi, J. Magn. Magn. Mater. **240**, 539 (2002)
13. G. Ausanio, V. Ianotti, I. Lanotte, M. Carbucicchio, M. Rateo, J. Magn. Magn. Mater. **226–230**, 1740 (2001)
14. R. Brucas, H. Hafermann, M.I. Katsnelson, I.L. Soroka, O. Eriksson, B. Hjorvarsson, Phys. Rev. B **69**, 064411 (2004)
15. G. Beutier, G. van der Laan, K. Chesnel, A. Marty, M. Belakhovsky, S.P. Collins, E. Dudzik, J.C. Toussaint, B. Gilles, Phys. Rev. B **71**, 184436 (2005)
16. Y.S. Chun, K.M. Krishnan, J. Appl. Phys. **95**, 6858 (2004)
17. Y.Z. Wu, C. Won, A. Scholl, A. Doran, H.W. Zhao, X.F. Jin, Z.Q. Qiu, Phys. Rev. Lett. **93**, 117204 (2004)
18. M. Labrune, L. Belliard, Phys. Stat. Sol. (a) **174**, 483 (1999)
19. M. Labrune, A. Thiaville, Eur. Phys. J. B **23**, 17 (2001)
20. M. Labrune, M. Carbucicchio, J. Magn. Magn. Mater. **269**, 203 (2004)

21. U. Ebels, L.D. Buda, K. Ounadjela, P.E. Wigen, *Spin Dynamics in Confined Magnetic Stucture I* (Springer, New-York, 2002)
22. N. Vukadinovic, H. Le Gall, J. Ben Youssef, V. Gehanno, A. Marty, Y. Samson, B. Gilles, Eur. Phys. B **13**, 445 (2000)
23. O. Acher, C. Boscher, B. Brulé, G. Perrin, N. Vukadinovic, G. Suran, H. Joisten, J. Appl. Phys. **81**, 4057 (1997)
24. J. Ben Youssef, N. Vukadinovic, D. Billet, M. Labrune, Phys. Rev. B **69**, 174402 (2004)
25. N. Vukadinovic, O. Vacus, M. Labrune, O. Acher, D. Pain, Phys. Rev. Lett. **85** 2817 (2000)
26. N. Vukadinovic, M. Labrune, J. Ben Youssef, A. Marty, J.C. Toussaint, H. Le Gall, Phys. Rev. B **65**, 054403 (2002)
27. J.F. Cochran, B. Heinrich, A.S. Arrott, Phys. Rev. B **34**, 7788 (1986)
28. G.T. Rado, J.R. Weertman, J. Phys. Chem. Solids **11**, 315 (1959)
29. W.B. Zeper, H.W. van Kesteren, B.A.J. Jacobs, J.M.H. Spruit, J. Appl. Phys. **70**, 2264 (1991)
30. J. Pelzl, R. Meckenstock, D. Spoddig, F. Schreiber, J. Pflaum, Z. Frait, J. Phys.: Condens. Matter **15**, S451 (2003)
31. A. Layadi, J.O. Artman, B.O. Hall, R.A. Hoffman, C.L. Jeuren, D.J. Chakrabarti, D.A. Saunders, J. Appl. Phys. **64**, 5760 (1988)
32. F. Schreiber, J. Pflaum, Z. Frait, Th. Muhge, J. Pelzl, Solid State Commun. **93**, 965 (1995)
33. M. Hehn, S. Padovani, K. Ounadjela, J.P. Bucher, Phys. Rev. B **54**, 3428 (1996)
34. U. Ebels, L. Buda, K. Ounadjela, P.E. Wigen, Phys. Rev. B **63**, 174437 (2001)
35. N. Vukadinovic, IEEE Trans. Mag. **MAG-38**, 2508 (2002)
36. G. Asti, M. Carbucicchio, M. Ghidini, M. Rateo, G. Ruggiero, M. Soizi, F. D'orazio, F. Lucari, J. Appl. Phys. **87**, 6689 (2000)
37. Yu. Goryunov, N.N. Garif'yanov, G.G. Khaliullin, I.A. Garifullin, L.R. Tagirov, F. Schreiber, T. Muhge, H. Zabel, Phys. Rev. B **52**, 13450 (1995)
38. M.T. Johnson, P.J.H. Bloemen, F.J.A. den Broeder, J.J. de Vries, Rep. Prog. Phys. **59**, 1409 (1996)
39. B. Hoekstra, R.P. van Stapele, J.M. Robertson, J. Appl. Phys. **48**, 382 (1977)